

A study of topological characterization and symmetries for a quantum simulated Kitaev chain

Y R Kartik,^{1,2} Ranjith R Kumar,^{1,2} S Rahul,^{1,2} and Sujit Sarkar¹

¹*Poornaprajna Institute of Scientific Research, 4, Sadashivanagar, Bangalore-560 080, India.*

²*Graduate Studies, Manipal Academy of Higher Education, Madhava Nagar, Manipal-576104, India.*

(Dated: September 11, 2020)

An attempt is made to quantum simulate the topological classification, such as winding number, geometric phase and symmetry properties for a quantum simulated Kitaev chain. We find, α (ratio between the spin-orbit coupling and magnetic field) and the range of momentum space of consideration, which plays a crucial role for the topological classification. We show explicitly that the topological quantum phase transition does not occur at $k = 0$ limit for the quantum simulated Kitaev chain. We observe that the quasi-particle mass of the Majorana mode plays the significant role in topological quantum phase transition. We also show that the symmetry properties of simulated Kitaev chain is the same with original Kitaev chain. The exact solution of simulated Kitaev chain is given. This work provides a new perspective on new emerging quantum simulator and also for the topological state of matter.

Quantum simulation process is a very prominent field of research interest in present and foreseeable future. One aim of quantum simulation is to simulate a quantum system using a controllable laboratory system which underlines the same analytical models. Therefore it is possible to simulate a quantum system that can be neither efficiently simulated on a classical computer nor easily accessed experimentally¹⁻¹³. New, Emerging Quantum Simulators will support creative, cutting-edge research in science to uncover different physical phenomena. Hamiltonian engineering is one of the major part of the quantum simulation process to study the behaviour of the system. It should be possible to engineer a set of interactions with external field or between different particle with tunable strength^{12,13}.

Intrinsic topological superconductors are quite rare in nature. However, one can engineer topological superconductivity by inducing effective p-wave pairing in materials which can be grown in the laboratory. One possibility is to induce the proximity effect in topological insulators¹⁴; another is to use hybrid structures of superconductors and semiconductors^{15,16,17}. If the quantum simulators develop a hybrid system in a quantum nanowire which belongs to the same symmetry class as p-wave superconductor then the hybrid system shows the same topological properties. This is the main theme/idea that motivated the scientists to propose a number of platforms which fulfils the requirements to simulate this phase and also the experimentalists propose it.

In condensed matter physics, the Majorana fermion is an emergent quasi-particle zero-energy state¹⁸. The fundamental aspects of Majoranas and their non-Abelian braiding properties^{19,20} offer possible applications in quantum computation²¹⁻²⁴.

In the topological state, Majorana fermions exists and form the degenerate ground state which is separated from the rest of the spectrum by an energy gap. A system of spatially separated Majorana fermions could be used as a quantum computer that is immune to the tremendous obstacle faced. Experimental confirmation of the existence of Majorana fermions is a crucial step towards practical quantum computing. Very recently, there have been many evidence of experimental signature²⁵⁻²⁷ of Majorana fermions.

The author of Ref.25 have shown the evidence MZMs from the study of tunneling conductance of an InAs nanowire proximated by the s-wave superconductor. Wandj-Prage *et al.*²⁶ exhibited scanning tunneling which microscopy highlighted the presence of MZM localized at the system edge. The authors of Ref.27 have predicted the existence of Majorana fermion at both ends from the study of zero bias peak.

From the theoretical side, the simplest model for realizing Majorana zero mode (MZM) is the one dimensional spinless p-wave chain proposed by Kitaev¹⁸. Implementation of Kitaev model in practical reality proposed by Fu and Kane¹⁴. In their work, they predicted the presence of MZM as a result of proximity effect between the s-wave superconductor and the surface state of a strong topological superconductor.

The authors of Ref.15 and Ref.16 have outlined the necessary ingredients for engineering a nanowire device that should pairs of Majoranas. But the topological characterization in momentum space and symmetries for the quantum simulated Kitaev chain are still absent in the literature.

Motivation :

The physics of topological states of matter is the second revolution in quantum mechanics. How to quantum simulate this topological state of matter in practical reality through quantum simulation process is one of the most prominent task to the scientific community.

Kitaev¹⁸ proposed this model in the year 2010 for the prediction of Majorana fermion mode and topological phase transition for one dimensional system. In the present study, we derive and explain the following topological characterization in momentum space and its several consequences.

We study and find the topological quantum phase transition for the simulated Kitaev chain and the parametric relation between the quasiparticle mass and the chemical potential at the transition point.

We study the geometric phase of the simulated Kitaev chain and quantization condition and also make a comparison with the behaviour of geometric phase of original Kitaev chain.

Symmetries are essential for understanding and describing the physical world. The reason is that they give rise to the conservation laws of physics, lead to degeneracies, control the structure of matter, and dictate interactions. Symmetries require the laws of physics to be invariant under changes of redundant degrees of freedom equivalently. Symmetries are perceived as the key to natures secret²⁸.

Symmetries also play an important role in the topological state of matter. Therefore it is one of the challenge to study the symmetry properties of the simulated Kitaev chain. This equivalence of symmetries between the simulated Kitaev chain and original Kitaev chain is one of the hallmark of the quantum state engineering of the simulated model Hamiltonian. Apart from that we are able to produce results of exact solution for this simulated Kitaev

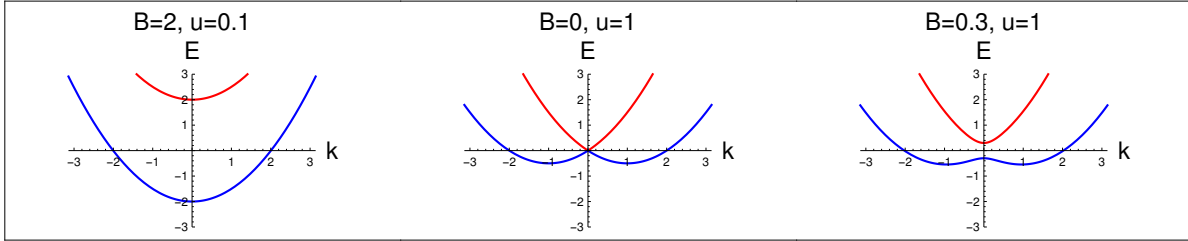


FIG. 1: (Colour online.) These figures show the normal state ($\Delta = 0$) energy dispersion of the quantum nano wire (eq.3) for different limits of B and u as depicted in the figures.

The left figure is for the Kitaev limit ($B \gg u$). The middle and right figure are respectively for topological insulator limit without and with magnetic field.

chain.

The experimentalists will be motivated with the results of this quantum simulated Kitaev chain. This work provides a new perspective on new emerging quantum simulator and also for the topological state of matter.

A brief outline of the generation of p-wave superconductivity and quantum simulated Kitaev chain: Engineering the simulated Hamiltonian

It is well known to all of us from the quantum simulation processes Hamiltonian engineering is one of the major challenge for the quantum simulation processes^{6,12,13}. Now we present a brief outline for the simulation of superconducting p-wave and then finally quantum simulated Kitaev chain. Here we consider a one dimensional quantum wire with Rashba spin orbit coupling (u), applied magnetic field (B) and couple to a s-wave superconductor with proximity induced pairing (Δ).

$$H_1 = \left(\frac{k^2}{2m} + uk\sigma_x - \mu \right) \tau_z - B\sigma_z + \Delta\tau_x. \quad (1)$$

Spin orbit coupling is along the x-direction which is perpendicular to the applied magnetic field (z-direction). The first term is the kinetic energy term, which leads to the topological superconducting phase that makes the difference with the topological insulator Hamiltonian. We explain the basic aspects of p-wave superconductivity and the quantum simulated Kitaev chain during the description of fig. 1. We also present the normal state dispersion in fig. 1. which present the three different situation of normal state in different figures. At first we neglect the spin-orbit coupling ($B \gg u$). Then the dispersion relation become, $\epsilon_k = \frac{k^2}{2m} \pm B$, i.e., we get the vertically shifted parabola for the up and down spin with a energy separation

$\sim 2B$, which we present it in the left figure of fig. 1.

In the middle figure is, two shifted parabola in presence of Rashba spin orbit interaction. This middle figure corresponds to topological insulator limit without Zeeman field. In this limit the dispersion is

$$\epsilon_k = \frac{k^2}{2m} \pm uk. \quad (2)$$

The right figure shows the dispersion curves in presence of both Zeeman field and spin orbit interaction ($u > B$). This is the topological insulator limit in the presence of magnetic field. It produce the gap at the crossing point of two parabola of size $2B$. In this limit the dispersion is

$$\epsilon_k = \frac{k^2}{2m} \pm \sqrt{u^2 k^2 + B^2}. \quad (3)$$

In presence of spin orbit coupling shifted the direction of the spin polarization of the energy spectrum parabola from the Zeeman direction with the tilting angle is proportional to k and as a consequence of it spin polarization is different (opposite) for the positive and negative momenta. When we consider the chemical potential inside the gap, we observe that there is a only one single left moving and single right moving electron and this limit is called helical spin configuration which finally leads to the spinless p-wave superconductors^{29–31}. We will see that the Zeeman field is not the sufficient to quantum simulate Kitaev chain but the spin-orbit interaction is also necessary to get the finite value of proximity induced superconductivity.

For finite Δ , the spectrum for constant μ, u, Δ and B is the following,

$$E_{\pm} = \pm \sqrt{B^2 + \Delta^2 + \epsilon_k^2 + uk^2 \pm 2\sqrt{B^2 \Delta^2 + B^2 \xi_k^2 + u^2 k^2 \xi_k^2}}. \quad (4)$$

Where $\xi_k = \frac{k^2}{2m} - \mu$. Near $k \sim 0$.

$$E_{\pm}(k \sim 0) = \pm \sqrt{B^2 + \Delta^2 + \mu^2 \pm 2B\sqrt{\Delta^2 + \mu^2}}. \quad (5)$$

It is very clear from the above expression that the gap closes at $k \sim 0$ at $B = \pm \sqrt{\Delta^2 + \mu^2}$. and the topological quantum phase transition occurs. It has claimed by the all studies in the previous literature of quantum nanowire^{15–17}. But we will prove explicitly that this relation does not hold for the Kitaev limit of the hybrid quantum nanowire and at the same time the transition does not occur at $k \sim 0$ but occurs for the consideration of finite range of momentum space during the integration. The derivation of simulated Kitaev chain is the

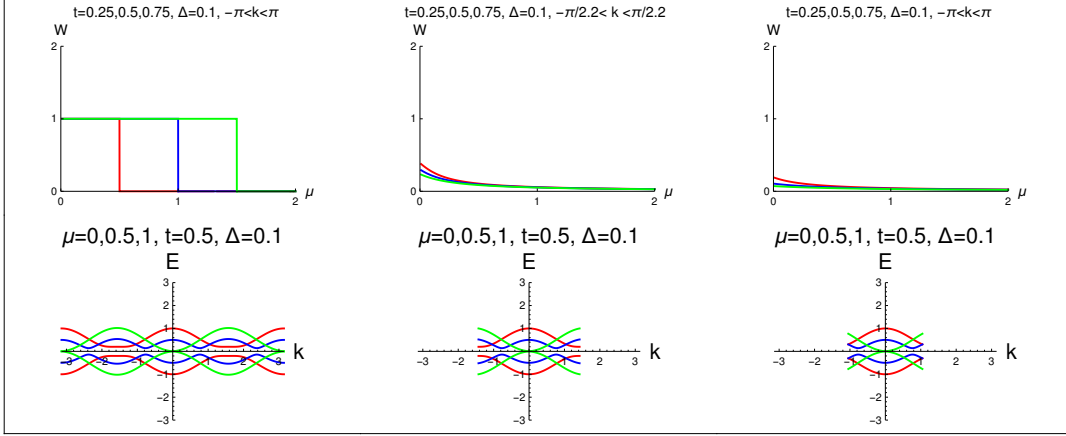


FIG. 2: (Colour online.) Figures of the upper panel show the variation of winding number with μ for the original Kitaev chain for different limit of momentum space as depicted in the figures. Each figures in the upper panel consists three curves for different values of $t = 0.25$ (red), $t = 0.5$ (blue) and $t = 0.75$ (green). Figures of the lower panel present the energy dispersion of the original Kitaev chain for the same parameter space and momentum space region of consideration. Each figures in the lower panel consists three curves for different values of $\mu = 0$ (red), $\mu = 0.5$ (blue) and $\mu = 0.75$ (green).

three-step processes. At first we consider the presence of magnetic field and the modification of kinetic energy (the left figure of the first panel). The second step is to find the effect of superconductivity on this dispersion. We show explicitly in the method section that the presence of spin-orbit interaction gives finite contribution p-wave superconductivity.

In this presentation Δ is always finite and less than B and u . As we derive the model Hamiltonian of the quantum nanowire in the Kitaev limit, i.e., the applied magnetic field (B) is much larger than the strength of spin-orbit coupling (u).

Finally we get the quantum simulated Hamiltonian in the following form (pls see the "Method" section for the detail derivation).

$$H = \left(\frac{k^2}{2m} - \mu\right)\tau_z - \frac{uk}{B}\Delta\tau_x. \quad (6)$$

The energy dispersion for this model Hamiltonian system is

$$\begin{aligned} E_k &= \sqrt{\left(\frac{k^2}{2m} - \mu\right)^2 + \left(\frac{uk\Delta}{B}\right)^2} \\ &= \sqrt{\left(\frac{k^2}{2m} - \mu\right)^2 + \alpha^2 k^2 \Delta^2}. \end{aligned} \quad (7)$$

Finally, we have obtained the quantum simulated Hamiltonian in the form of an Anderson pseudo-spin Hamiltonian³² as we obtain for the Kitaev chain¹⁸. The effect of p-wave pairing strength of the proximity coupled quantum wire is $\frac{uk\Delta}{B}$. Thus it is very clear that the effect of spin orbit coupling has the effect to generate the p-wave pairing. The most important contribution of quantum wire with high magnetic field emerges the topological superconducting phase. In the present study we define a parameter $\alpha = \frac{u}{B}$, i.e, the ratio between the strength of spin-orbit coupling and the applied magnetic field and the other parameter is the consideration of momentum space region, which is less than the full Brillouin zone. We will see that these two parameters play the role for the topological quantization for the quantum simulated Kitaev chain.

Results:

Topological characterization in momentum space

(A). Results of topological invariant number with physical explanations

At first we present the results of Kitaev chain for benchmarking the results of quantum simulated Kitaev chain (eq. 6).

$$H_1 = -t \sum_{i=1}^{N-1} (c_i^\dagger c_i + h.c) + \sum_{i=1}^{N-1} (|\Delta| c_i c_{i+1} + h.c) - \mu \sum_{i=1}^N c_i^\dagger c_i. \quad (8)$$

One can also write the Hamiltonian as,

$$h(k) = \vec{\chi}(k) \cdot \vec{\tau}, \quad (9)$$

where $\vec{\tau}$ are Pauli matrices which act in the particle-hole basis, and $\chi_x(k) = 0$, $\chi_y(k) = 2\Delta \sin k$ and $\chi_z(k) = -2t \cos k - \mu$. It is convenient to define this topological invariant quantity using the Anderson pseudo-spin approach³².

$$\vec{\chi}(k) = \Delta(k) \vec{y} + (\epsilon_k - \mu) \vec{z}. \quad (10)$$

It is very clear from the analytical expression that the pseudo spin defined in the $y-z$ plane,

$$\hat{\chi}(k) = \frac{\vec{\chi}(k)}{|\vec{\chi}(k)|} = \cos(\theta_k) \hat{y} + \sin(\theta_k) \hat{z}. \quad (11)$$

$$\theta_k = \tan^{-1}(-(2t \cos k + \mu)/(2\Delta \sin k)). \quad (12)$$

The energy dispersion is

$$E_k = \sqrt{\chi_y^2(k) + \chi_z^2(k)}. \quad (13)$$

winding number is only an integer number and ,therefore, can not vary with smooth deformation of the Hamiltonian as long as the quasi-particle gap remains finite. At the point of topological phase transition the winding number changes discontinuously.

The analytical expression for winding number (W) for Kitaev chain is

$$W = \left(\frac{1}{2\pi}\right) \int_{-\pi}^{\pi} \left(\frac{d\theta_k}{dk}\right) dk = \left(\frac{1}{2\pi}\right) \int_{-\pi}^{\pi} \frac{2\Delta(2t + \mu \cos k)}{(\mu + 2t \cos k)^2 + 4\Delta^2 \sin^2 k} dk. \quad (14)$$

Now we write quantum simulated Kitaev chain Hamiltonian in the matrix form after the change of basis, one can also write the above Hamiltonian in the following form.

$$H_s = \begin{pmatrix} \chi_{sz}(k) & i\chi_{sy}(k) \\ -i\chi_{sy}(k) & -\chi_{sz}(k) \end{pmatrix}. \quad (15)$$

$$\chi_{sz}(k) = \frac{k^2}{2m} - \mu; \quad \chi_{sy}(k) = \frac{uk\Delta}{B}. \quad \chi_{sz}(k) = \chi_z(-k), \quad \chi_{sy}(k) = -\chi_{sy}(-k).$$

$$\theta_{sk} = \tan^{-1}(\chi_{sz}(k)/\chi_{sy}(k)). \quad (16)$$

The analytical expression of winding number for simulated Kitaev chain is (we use the first expression of eq.14 to derive the winding number)

$$W_s = \frac{1}{2\pi} \int_{-\pi/a}^{\pi/a} \frac{2Bmu\Delta(k^2 + 2m\mu)dk}{4k^2m^2u^2\Delta^2 + B^2(k^2 - 2m\mu)^2} = \frac{1}{2\pi} \int_{-\pi/a}^{\pi/a} \frac{2m\alpha\Delta(k^2 + 2m\mu)dk}{4k^2m^2\alpha^2\Delta^2 + (k^2 - 2m\mu)^2}, \quad (17)$$

where $\alpha = \frac{u}{B}$.

At first we present the results of original Kitaev chain for the completeness of the study because we compare the results of simulated Kitaev chain with the results of original Kitaev chain.

Fig. 2 consists of two panels. The upper panel is for the variation of winding number with the chemical potential (μ) and the lower panel is for the energy dispersion (eq. 13) for the same parameter space of winding number study.

We observe that the topological quantum phase transition occurs at $\mu = 2t$, when we consider the full Brillouin zone boundary (B.Z) in the momentum space. We also observe from the study of second and third figure of the upper panel that there is no topological quantum phase transition for the same parameter space, for these figures we have not considered the momentum space regime for full B.Z. We observe that in lower panel, energy gap disappears for topological quantum phase transition when we consider the full B.Z in the momentum

space (left figure of lower panel) otherwise there is no gap closing.

In fig.3, we present the variation of winding number with chemical potential for the different region of the momentum space. We find the topological quantum phase transition occurs at $\mu = 1/m$. This can be explained in the following way:

For the small momentum one can expand the cosine term as $1 - k^2/2$. Therefore one can write the hopping integral as $t = 1/2m$ by using the dispersion relation. The parametric relation for topological quantum transition is $\mu = 2t = 1/m$. It reveals from this figure that the topological quantization has started to work for the integration region $-\frac{\pi}{2} < k < \frac{\pi}{2}$. But we observe that the topological quantum phase transition occurs for the simulated Kitaev chain occurs at $\mu = 1/m$ for the consideration of momentum space, $-\frac{\pi}{2.2} < k < \frac{\pi}{2.2}$, we term this region of momentum space as an effective Brillouin zone to quantum simulate the topological state of matter. Here we consider the value of $\Delta = 0.1$. We justify this value of Δ in the description of exact solution (eq. 23). Each figure consists of three curves for different values of α . We observe that as the value of the α increase, i.e., the strength of the spin orbit interaction increases, the quantization condition for the topological quantum phase transition disappears. Thus to obtain the topological quantization for the simulated Kitaev chain the magnetic field should be much higher than the spin-orbit coupling.

This prediction is consistent with our consideration for the smaller values of α during the quantum state engineering of simulated Kitaev chain.

Fig.4, shows the variation of winding number (W) with the quasi-particle mass. We find the same parametric relation for the topological quantum phase transition, we also observe that this transition occurs at $\mu = 1/m$.

We also observe that as we approach smaller range of momentum space consideration, winding number drops sharply and touch the base line, i.e., in the limit $k = 0$, there is no topological quantum phase transition.

Why the winding number become zero in the momentum regime becomes zero

$$\tilde{H} = -\mu\tau_z + \frac{uk\Delta}{B}\tau_x. \quad (18)$$

This is the Anderson pseudo spin Hamiltonian for the quantum simulated Kitaev chain. We

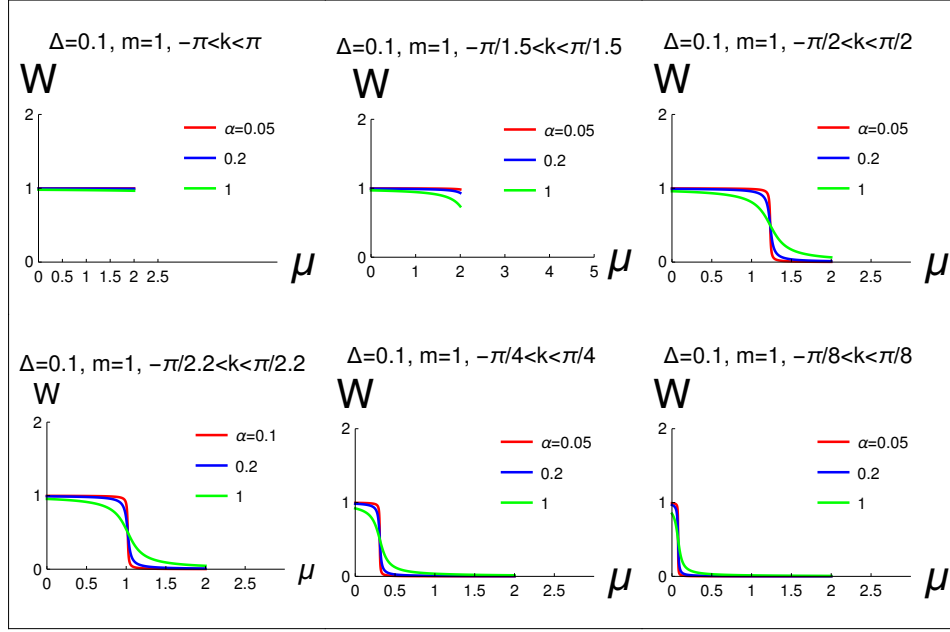


FIG. 3: (Colour online.) These figures show the variation of winding number with chemical potential for different region of momentum space consideration as depicted in the figures. Each figure consist of three curves for different values of α as depicted in the figures. Here we consider $\Delta = 0.1$ and $m = 1$.

now show explicitly that this model Hamiltonian has no topological phase transition.

$$\tilde{H} = \begin{pmatrix} -\mu & i\frac{uk\Delta}{B} \\ -i\frac{uk\Delta}{B} & \mu \end{pmatrix}. \quad (19)$$

Finally we obtain, winding number for the Hamiltonian (eq. 17) as

$$W_s = \frac{1}{2\pi} \int_{-\pi/a}^{\pi/a} \frac{u\Delta\mu dk}{k^2 u^2 \Delta^2 + B^2 \mu^2} \quad (20)$$

$$W_s = \left(\frac{1}{2\pi}\right) \frac{\mu}{u\Delta} \int_{-\pi/a}^{\pi/a} \frac{dk}{k^2 + \beta^2}, \quad (21)$$

Where $\beta = \frac{B^2 \mu^2}{u^2 \Delta^2}$.

$$W_s = \left(\frac{1}{2\pi}\right) \frac{u\Delta(B - \mu)}{u^2 \Delta^2} \text{Arctan}(k/\beta). \quad (22)$$

Thus it is clear from the above expression of simulated winding number that it goes to zero as the momentum goes to zero.

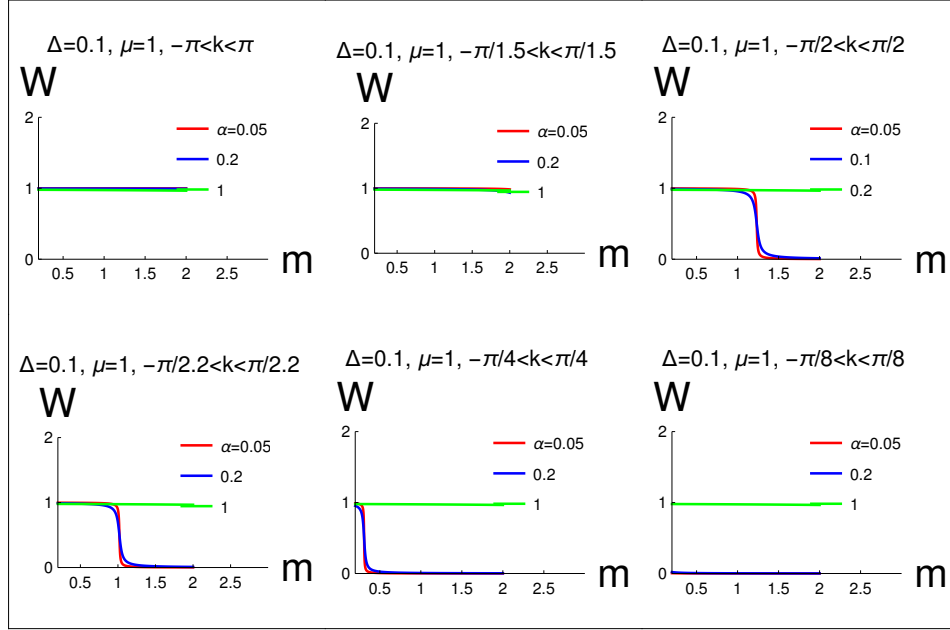


FIG. 4: (Colour online.) These figures show the variation of winding number with m for different region of momentum space consideration as depicted in the figures. Each figure consists of three curves for different values of α as depicted in the figures. Here we consider

$$\Delta = 0.1 \text{ and } \mu = 1.$$

In fig.5, we present the dispersion for the simulated Kitaev chain (eq.7). This figure consists of two different panels for the different values of momentum space region. For the upper panel: the left, middle and right are respectively for the momentum space region $-\pi < k < \pi$, $-\pi/1.5 < k < \pi/1.5$, and $-\pi/2.5 < k < \pi/2.5$. For the right panel: the left, middle and right are respectively for the momentum space region $-\pi/2.2 < k < \pi/2.2$, $-\pi/2.5 < k < \pi/2.5$, and $-\pi/2.5 < k < \pi/2.5$. It reveals from this study the gap between the two bands close at the point $k = \pm\pi/2.2$. Thus the system shows the topological quantum phase transition for this value of k .

In fig.6, we present the dispersion for the simulated Kitaev chain (eq.4) for two different values of u . One is $u = 2$ (left figure) and the other is $u = 0.2$ (right figure). Each figures consists four curves, two them we present in red colour and the other two present by blue colour. The upper and lower red curves are respectively for the dispersion for plus and minus in front of square root of eq.4. The upper and lower blue curves are respectively for the dispersion for plus and minus sign inside of square root of eq.4.

It reveals from these figures that for the higher values of u , there is always gap in the

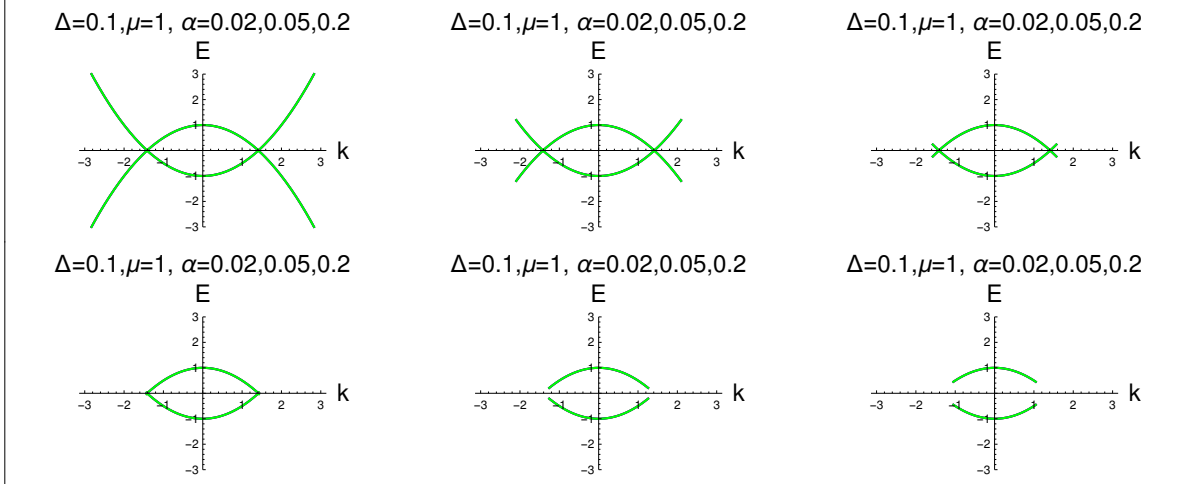


FIG. 5: (Colour online.) These figures show the dispersion of simulated Kitaev chain (eq.7) with k and the range of momentum space consideration for the upper panel are $-\pi < k < \pi$ (left), $-\pi/1.5 < k < \pi/1.5$ (middle) and $-\pi/2 < k < \pi/2$ (right), and for lower panel are $-\pi/2.2 < k < \pi/2.2$ (left), $-\pi/2.5 < k < \pi/2.5$ (middle) and $-\pi/3 < k < \pi/3$ (right). Each figures consists of three different curves for different values of α as depicted in the figures. But all of the curves are coincide and finally green colour appears.

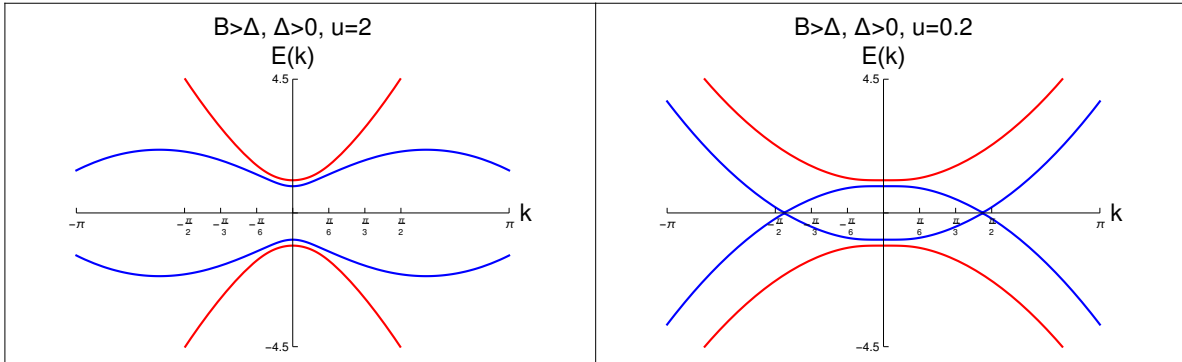


FIG. 6: (Colour online.) These figures show the dispersion for the different limit of eq. 4 (we discuss explicitly in the main text of the manuscript), left and right figures are for $\alpha = 2$, and $\alpha = 0.2$ respectively. Here we consider $B=1$ and $\Delta = 0.1$.

dispersion spectrum but for the lower values of $u = 0.2$ the lower and upper band touches at $\pm k = \pi/2.2$.

Exact solution of simulated Kitaev chain

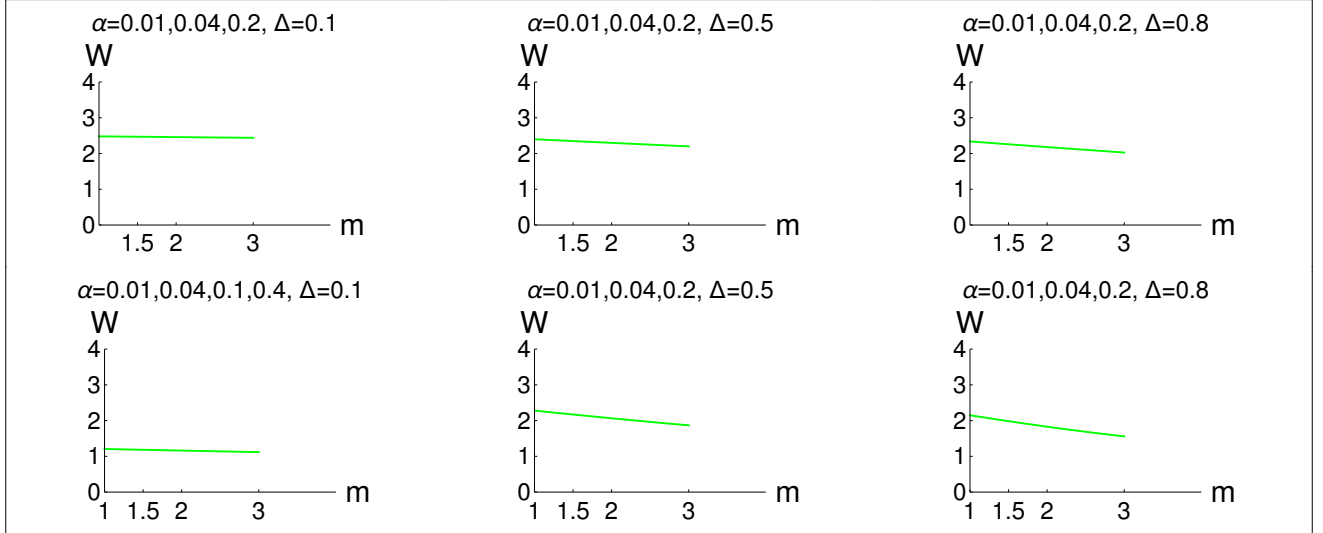


FIG. 7: (Colour online.) These figures show the results of exact solution (eq. 23). This figure consists of two panels for different region of momentum space of consideration. The upper and lower panels are for the momentum space region $-\pi < k < \pi$ and $-\pi/2.2 < k < \pi/2.2$ respectively. Each figures consists of three different curves for different values of α as depicted in the figures. But all of the curves are coincide and finally green colour appears.

It is well known that the Kitaev chain has the exact solution for $\mu = 0$, for $\Delta = t$. For this limit, system is always in the topological state with out any transition. One can understand this constant topological state with out any transition for $\mu = 0$ from the parametric relation ($\mu = 2t$) also.

Therefore it is also a chalange to check the existence of exact solution for the simulated Kitaev chain. The exact solution of winding number is

$$W_{exact} = \frac{1}{\alpha\pi} \text{Arccot}\left(\frac{2m\alpha\Delta}{a\pi}\right). \quad (23)$$

In fig. 7, we present the exact result of W with the variation of m . Upper and lower panels of this figure are for $-\pi < k < \pi$ and $-\pi/2.2 < k < \pi/2.2$ respectively. Each panel consists of three figures for different values of Δ . It reveals from this study that there is no topological state with winding number one for the upper panel. In the lower panel, we observe that system is in the topological state of matter with winding number very close to unity for the value of $\Delta = 0.1$. We observe that for higher values of Δ , the topological state is no more constant with unity winding number with m . Therefore, it is clear from from

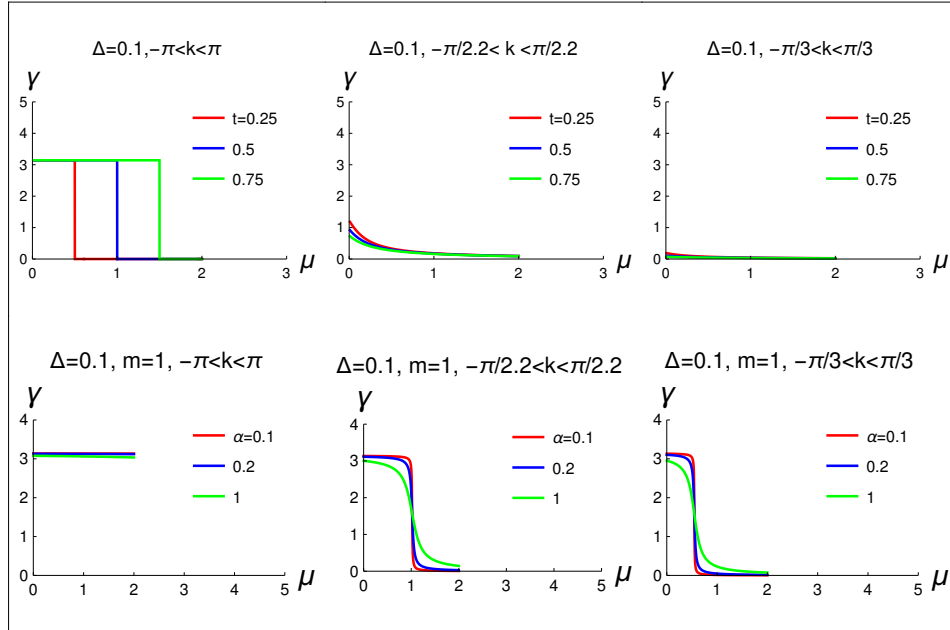


FIG. 8: (Colour online.) These figures show the variation of γ with μ . This figure consists of two panels, upper and lower panels are respectively for the results of the original Kitaev chain and simulated Kitaev chain. The parameter space of these figures are depicted in the figures and also different region of momentum space of consideration.

this results that we are also reproduce the exact solution of the Kitaev chain for smaller values of Δ . This is also one of the most success of this quantum simulated Kitaev chain.

Results of geometric phase with physical explanation

At first we describe very briefly the basic aspect of geometric phase. During the adiabatic time evolution of the system, the state vector acquires an extra phase over the dynamical phase, $|\psi(R(t))\rangle = e^{\alpha_n} |\phi(R(t))\rangle$, where $\alpha_n = \theta_n + \gamma_n$. $\theta_n (= \frac{-1}{\hbar} \int_0^t E_n(\tau) d\tau)$ and γ_n are the dynamical and geometric phases respectively. For a system is given to the cyclic evolution described by a closed curve. It is evident from the analytical expression of Berry phase that it depends on the geometry of the parameter and loop (C) therein.

$$\gamma_n(C) = i \int_C \langle \phi(x) | \nabla | \phi(x) \rangle dx.$$

The geometric (Zak) phase is an important concept for the topological characterization of low dimensional quantum many body system^{13,33,34}. Zak has considered the one dimensional Brillouin zone and the cyclic parameter is the crystal momentum (k). The geometric phase

in the momentum space is defined as

$$\gamma_n = \int_{-\pi}^{\pi} dk \langle u_{n,k} | i\partial_k | u_{n,k} \rangle, \quad (24)$$

where $|u_{n,k}\rangle$ is the Bloch states which are the eigenstates of the n^{th} band of the Hamiltonian. The simulated Kitaev chain possesses Z type topological invariant and also the anti-unitary particle hole symmetry (please see the ‘‘Symmetry’’ section for the detailed symmetry operations). For this system, the analytical expressions of the Zak phase^{13,33,34} is

$$\gamma = W\pi \quad \text{mod } (2\pi). \quad (25)$$

In fig.8, we present results of geometric phase. In the upper and lower panel, we present the geometric phase for the original Kitaev chain and simulated Kitaev chain with chemical potential, respectively. The figures in the upper and lower panels are for the different values of momentum space region consideration as depicted in figures. Each figures in the upper panel consists of three curves for different values of hopping integral (t), and they satisfy the quantization from finite value $\gamma(= \pi)$ to zero, i.e, the system drives from the topological state of matter to the non-topological state. It is very clear from this figure that the quantization condition of γ appears when we consider the full B.Z of the momentum space. Each figures in lower panels consists of three curves for different values of α . It is also clear from this study that as we increase the value of α the quantization condition for the γ smeared out and there is no topological quantum phase transition for the simulated Kitaev chain.

It reveals from the study of lower panel that γ shows the same behaviour of original Kitaev chain when we consider the momentum space region $-\pi/2.2 < k < \pi/2.2$. For the original Kitaev chain the Bloch state traverse in whole B.Z but for the simulated Kitaev chain Bloch state traverse in the reduced momentum space as we see from the dispersion. For the consideration of momentum space region $-\pi/2.2 < k < \pi/2.2$ for the simulated Kitaev chain, gives the same parametric relation of original Kitaev chain for the topological phase transition.

Symmetry presentation of simulated Kitaev chain

Among the vast variety of topological phases one can identify an important class called symmetry protected topological (SPT) phase, where two quantum states have distinct topological properties protected by certain symmetry. Under this symmetry constraint, one

can define the topological equivalent and distinct classes. Hamiltonians which are invariant under the continuous deformation into one another preserving certain symmetries are the topological equivalent classes.

Different SPT states can be well understood with the local (gauge) non-spatial symmetries such as, time reversal (TR), particle-hole (PH) and chiral. In general non interacting Hamiltonians can be classified in terms of symmetries into ten different symmetry classes^{35–38}. A particular symmetry class of a Hamiltonian is determined by its invariance under time-reversal, particle-hole and chiral symmetries. Apart from that we also study the parity (P) symmetry, parity-time (PT) symmetry, charge conjugation-parity-time (CPT) symmetry, CP symmetry and CT symmetry. In this section, we present symmetry properties of the simulated Kitaev chain and also to check how much it is equivalent with original Kitaev chain.

Here we present the final results, of the symmetry operations for this quantum simulated model Hamiltonian. The detail derivation is relegated to the "Method" section.

Time-reversal symmetry

Time-reversal symmetry operation is $\hat{\Theta}$.

$$\hat{\Theta}^\dagger H_{BdG}(k) \hat{\Theta} = H(k).$$

Thus, the Hamiltonian obeys time-reversal symmetry.

Charge-conjugation symmetry

This symmetry operator is $\hat{\Xi}$.

$$\hat{\Xi}^\dagger \hat{H}(k) \hat{\Xi} = (\sigma_x \hat{K})^\dagger \hat{H}(k) (\sigma_x \hat{K}) = \hat{K}^\dagger \sigma_x \hat{H}(k) \sigma_x \hat{K} = -\hat{H}(k)$$

Thus, the Hamiltonian obeys charge-conjugation symmetry.

Chiral symmetry

This symmetry operator is given by, $\hat{\Pi}$.

$$\hat{\Pi}^\dagger H_{BdG}(k) \hat{\Pi} = \sigma_x H_{BdG}(k) \sigma_x = -\hat{H}(k)$$

Thus, the Hamiltonian also obeys chiral symmetry.

Parity symmetry $PH(k)P^{-1} = \sigma_z H(k) \sigma_z = H(-k)$

Thus, the Hamiltonian obeys parity symmetry.

PT symmetry

$$PTH(k)(PT)^{-1} \neq H(k)$$

Thus the Hamiltonian does not obeys PT symmetry.

CP symmetry $CPH(k)(CP)^{-1} = \sigma_x K \sigma_z H(k) \sigma_z K^{-1} \sigma_x = -H(-k)$

Thus, the Hamiltonian obeys CP symmetry.

CT symmetry

$$CTH(k)(CT)^{-1} = \sigma_x H(k) \sigma_x = -H(k)$$

Thus, the Hamiltonian obey the CT symmetry.

CPT symmetry

$$\alpha H(k) \alpha^{-1} = \sigma_x \sigma_z K H(k) K^{-1} \sigma_z \sigma_x \neq -H(k)$$

This simulated Hamiltonian does not obey CPT symmetry.

Thus it is clear from this symmetry study that the symmetry, properties of the simulated Kitaev chain and the Kitaev chain are the same³⁸.

Discussions:

We have studied quantum simulated Kitaev chain for a quantum nanowire with hybrid structure. We have presented results for topological quantization and geometric phase of this simulated Kitaev chain. We have shown explicitly that topological characterization in momentum space depends on two factors, one is the relative strength between the spin-orbit interaction and magnetic field and the other is the consideration of momentum space region. We have shown that the symmetry of the quantum simulated Kitaev chain is the same with the original Kitaev chain. We have also presented the exact solution. This work provides a new perspective on new emerging quantum simulator and also for the topological state of matter.

Method

(A). Derivation of Kitaev chain for a quantum nanowire

Kitaev limit can be achieved in the presence of strong magnetic field. Energy spectrum split in to two parabolic spectrum for two different spins species, up and down and the chemical potential is inside the gap. The lower energy state is for the up spin. The kinetic energy contribution is

$$H_{kin} = \left(\frac{k^2}{2m} - (B + \mu) \right) \tau_z. \quad (26)$$

At first we introduce six important operators.

$$\tau_x = \begin{pmatrix} 0 & 0 & 1 & 0 \\ 0 & 0 & 0 & 1 \\ 1 & 0 & 0 & 0 \\ 0 & 1 & 0 & 0 \end{pmatrix}, \tau_y = \begin{pmatrix} 0 & 0 & -i & 0 \\ 0 & 0 & 0 & -i \\ i & 0 & 0 & 0 \\ 0 & i & 0 & 0 \end{pmatrix}, \tau_z = \begin{pmatrix} 1 & 0 & 0 & 0 \\ 0 & 1 & 0 & 0 \\ 0 & 0 & -1 & 0 \\ 0 & 0 & 0 & -1 \end{pmatrix}$$

Similarly there are operators σ_x, σ_y and σ_z are acting on the spin space.

$$\sigma_x = \begin{pmatrix} 0 & 1 & 0 & 0 \\ 1 & 0 & 0 & 0 \\ 0 & 0 & 0 & 1 \\ 0 & 0 & 1 & 0 \end{pmatrix}, \sigma_y = \begin{pmatrix} 0 & -i & 0 & 0 \\ i & 0 & 0 & 0 \\ 0 & 0 & 0 & -i \\ 0 & 0 & i & 0 \end{pmatrix}, \sigma_z = \begin{pmatrix} 1 & 0 & 0 & 0 \\ 0 & -1 & 0 & 0 \\ 0 & 0 & 1 & 0 \\ 0 & 0 & 0 & -1 \end{pmatrix}$$

These operators τ_x, τ_y and τ_z are acting on the particle-hole space. Similarly there are operators σ_x, σ_y and σ_z are acting on the spin space.

These six operators are mainly used for the calculations for the topological state of matter. Here we are simulating the Kitaev model for the spin less fermion system, therefore we will use the operators τ 's.

In the next step, one can consider the pairing term. The low energy space of BdG equation is spanned by the spin up electron.

$$|e\rangle = (1, 0, 0, 0)^T \text{ and the spin up hole } |h\rangle = (0, 0, 0, 1)^T.$$

In this subspace of energy there is no pairing term. The matrix elements, $\langle e|\Delta\tau_x|e\rangle = \langle h|\Delta\tau_x|e\rangle = \langle e|\Delta\tau_x|h\rangle = \langle h|\Delta\tau_x|h\rangle = 0$.

$$\begin{aligned} \langle h|\Delta\tau_x|h\rangle &= \Delta(0, 0, 0, 1) \begin{pmatrix} 0 & 0 & 1 & 0 \\ 0 & 0 & 0 & 1 \\ 1 & 0 & 0 & 0 \\ 0 & 1 & 0 & 0 \end{pmatrix} (0, 0, 0, 1)^T \\ \langle h|\Delta\tau_x|h\rangle &= \Delta(0, 0, 0, 1) \begin{pmatrix} 0 & 0 & 1 & 0 \\ 0 & 0 & 0 & 1 \\ 1 & 0 & 0 & 0 \\ 0 & 1 & 0 & 0 \end{pmatrix} \begin{pmatrix} 0 \\ 0 \\ 1 \\ 0 \end{pmatrix} = \Delta(0, 0, 0, 1) \begin{pmatrix} 0 \\ 1 \\ 0 \\ 0 \end{pmatrix} = 0 \\ \langle e|\Delta\tau_x|e\rangle &= \Delta(1, 0, 0, 0) \begin{pmatrix} 0 & 0 & 1 & 0 \\ 0 & 0 & 0 & 1 \\ 1 & 0 & 0 & 0 \\ 0 & 1 & 0 & 0 \end{pmatrix} \begin{pmatrix} 1 \\ 0 \\ 0 \\ 0 \end{pmatrix} = \Delta(1, 0, 0, 0) \begin{pmatrix} 0 \\ 0 \\ 1 \\ 0 \end{pmatrix} = 0 \end{aligned}$$

$$\langle e|\Delta\tau_x|h\rangle = \Delta(1,0,0,0) \begin{pmatrix} 0 & 0 & 1 & 0 \\ 0 & 0 & 0 & 1 \\ 1 & 0 & 0 & 0 \\ 0 & 1 & 0 & 0 \end{pmatrix} \begin{pmatrix} 0 \\ 0 \\ 0 \\ 1 \end{pmatrix} = 0$$

$$= \langle h|\Delta\tau_x|e\rangle$$

Therefore it reveals from this study that the spin singlet pairing can not induced proximity superconductivity in a perfectly spin polarized system. This is also physically consistent because the spin singlet is possible only when the band is populated with up and down spin state.

Therefore to get the finite contribution of superconductivity, we must have to be consider the spin orbit coupling modified the energy spectrum and populated the both up and down spin.

Now the spinor become modified $|e\rangle = (1, -\frac{uk}{2B}, 0, 0)^T$ and the spin up hole $|h\rangle = (0, 0, -\frac{uk}{2B}, 1)^T$.

In this subspace, one can obtain $\langle h|\Delta\tau_x|e\rangle = \langle e|\Delta\tau_x|h\rangle = -\frac{uk}{B}\Delta$, other matrix elements are zero.

$$\langle e|\Delta\tau_x|e\rangle = \Delta(0, \frac{-uk}{2B}, 0, 0) \begin{pmatrix} 0 & 0 & 1 & 0 \\ 0 & 0 & 0 & 1 \\ 1 & 0 & 0 & 0 \\ 0 & 1 & 0 & 0 \end{pmatrix} \begin{pmatrix} 0 \\ \frac{-uk}{2B} \\ 0 \\ 0 \end{pmatrix} = \Delta(0, \frac{-uk}{2B}, 0, 0) \begin{pmatrix} 0 \\ 0 \\ 1 \\ -\frac{uk}{2B} \end{pmatrix}$$

$$= 0 = \langle h|\Delta\tau_x|h\rangle$$

$$\langle h|\Delta\tau_x|e\rangle = \Delta(0, 0, \frac{-uk}{2B}, 0) \begin{pmatrix} 0 & 0 & 1 & 0 \\ 0 & 0 & 0 & 1 \\ 1 & 0 & 0 & 0 \\ 0 & 1 & 0 & 0 \end{pmatrix} \begin{pmatrix} 0 \\ \frac{-uk}{2B} \\ 0 \\ 0 \end{pmatrix} = \Delta(0, 0, \frac{-uk}{2B}, 0) \begin{pmatrix} 0 \\ 0 \\ 1 \\ -\frac{uk}{2B} \end{pmatrix}$$

$$= -\Delta\frac{uk}{2B} = \langle e|\Delta\tau_x|h\rangle$$

Therefore the final form of the model Hamiltonian is

$$H \simeq (\frac{k^2}{2m} - \mu)\tau_z - \frac{uk}{B}\Delta\tau_x$$

. This is the analogous form of the BdG Hamiltonian of a spinless p-wave superconductor with the effective pairing $\Delta_{eff} = \frac{u\Delta}{B}$. Therefore we conclude that effective p-wave pairing is

present due to the presence of spin orbit coupling and become weak when Zeeman field is large.

(B). An extensive derivation of symmetries for simulated Kitaev chain

Time-reversal symmetry

Time-reversal symmetry operation is $\hat{\Theta}$.

$$\hat{\Theta}^\dagger \hat{H}_{BdG}(k) \hat{\Theta} = \hat{K}^\dagger \hat{H}_{BdG}(k) \hat{K}. \quad \hat{\Theta}^\dagger \hat{H}_{BdG}(k) \hat{\Theta} = \hat{K} \begin{bmatrix} \chi_z(k) & i\chi_y(k) \\ -i\chi_y(k) & -\chi_z(k) \end{bmatrix} \hat{K} = H(k)$$

$\chi_z(k) = \frac{k^2}{2m} - \mu$, $\chi_y(k) = \alpha(= u/B)\Delta k$, Thus the Hamiltonian obeys time reversal symmetry.

We use the properties of $\chi_z(k) = \chi_z(-k)$ and $\chi_y(k) = -\chi_y(-k)$.

Charge-conjugation symmetry

This symmetry operator is $\hat{\Xi}$.

$$\begin{aligned} \hat{\Xi}^\dagger \hat{H}(k) \hat{\Xi} &= (\sigma_x \hat{K})^\dagger \hat{H}(k) (\sigma_x \hat{K}) = \hat{K}^\dagger \sigma_x \hat{H}(k) \sigma_x \hat{K} \\ \hat{\Xi}^\dagger \hat{H}(k) \hat{\Xi} &= \hat{K}^\dagger \begin{pmatrix} 0 & 1 \\ 1 & 0 \end{pmatrix} \begin{pmatrix} \chi_z(k) & i\chi_y(k) \\ -i\chi_y(k) & -\chi_z(k) \end{pmatrix} \begin{pmatrix} 0 & 1 \\ 1 & 0 \end{pmatrix} \hat{K} \\ \hat{\Xi}^\dagger \hat{H}(k) \hat{\Xi} &= \hat{K} \begin{pmatrix} -\chi_z(k) & -i\chi_y(k) \\ i\chi_y(k) & \chi_z(k) \end{pmatrix} \hat{K} = \begin{pmatrix} -\chi_z(k) & -i\chi_y(k) \\ i\chi_y(k) & \chi_z(k) \end{pmatrix} = -\hat{H}(k) \end{aligned}$$

Thus, the Hamiltonian obeys charge-conjugation symmetry.

Chiral symmetry

This symmetry operator is given by, $\hat{\Pi}$.

$$\begin{aligned} \hat{\Pi}^\dagger \hat{H}_{BdG}(k) \hat{\Pi} &= \sigma_x \hat{H}_{BdG}(k) \sigma_x \\ \hat{\Pi}^\dagger \hat{H}(k) \hat{\Pi} &= \begin{pmatrix} 0 & 1 \\ 1 & 0 \end{pmatrix} \begin{pmatrix} \chi_z(k) & i\chi_y(k) \\ -i\chi_y(k) & -\chi_z(k) \end{pmatrix} \begin{pmatrix} 0 & 1 \\ 1 & 0 \end{pmatrix} = -H(k) \end{aligned}$$

Thus, the Hamiltonian also obeys chiral symmetry.

Parity symmetry

$$\begin{aligned} PH(k)P^{-1} &= \sigma_z H(k) \sigma_z \\ &= \begin{pmatrix} 1 & 0 \\ 0 & -1 \end{pmatrix} \begin{pmatrix} \chi_z(k) & i\chi_y(k) \\ -i\chi_y(k) & \chi_z(k) \end{pmatrix} \begin{pmatrix} 1 & 0 \\ 0 & -1 \end{pmatrix} = H(-k) \end{aligned} \quad (27)$$

Thus, the Hamiltonian obeys parity symmetry.

PT symmetry

$$\begin{aligned}
PTH(k)(PT)^{-1} &= \sigma_z KH(k)K^{-1}\sigma_z \\
&= \sigma_z H(k)\sigma_z \\
&= \begin{pmatrix} 1 & 0 \\ 0 & -1 \end{pmatrix} \begin{pmatrix} \chi_z(k) & i\chi_y(k) \\ -i\chi_y(k) & -\chi_z(k) \end{pmatrix} \begin{pmatrix} 1 & 0 \\ 0 & -1 \end{pmatrix} \\
&= \begin{pmatrix} \chi_z(k) & -i\chi_y(k) \\ i\chi_y(k) & -\chi_z(k) \end{pmatrix} \neq H(k)
\end{aligned} \tag{28}$$

Thus the Hamiltonian does not obeys PT symmetry.

CP symmetry

$$\begin{aligned}
CPH(k)(CP)^{-1} &= \sigma_x K \sigma_z H(k) \sigma_z K^{-1} \sigma_x \\
&= \sigma_x K \begin{pmatrix} 1 & 0 \\ 0 & -1 \end{pmatrix} \begin{pmatrix} \chi_z(k) & i\chi_y(k) \\ -i\chi_y(k) & -\chi_z(k) \end{pmatrix} \begin{pmatrix} 1 & 0 \\ 0 & -1 \end{pmatrix} K^{-1} \sigma_x \\
&= \sigma_x K \begin{pmatrix} \chi_z(k) & -i\chi_y(k) \\ i\chi_y(k) & -\chi_z(k) \end{pmatrix} K^{-1} \sigma_x = -H(-k)
\end{aligned} \tag{29}$$

Thus, the Hamiltonian obeys CP symmetry.

CT symmetry

$$CTH(k)(CT)^{-1} = \sigma_x H(k) \sigma_x = -H(k) \tag{30}$$

Thus, the Hamiltonian obey the CT symmetry.

CPT symmetry

$$\begin{aligned}
\alpha H(k) \alpha^{-1} &= \sigma_x \sigma_z KH(k)K^{-1}\sigma_z \sigma_x \\
&= \begin{pmatrix} 0 & 1 \\ -1 & 0 \end{pmatrix} \neq -H(k)
\end{aligned} \tag{31}$$

- [1] Richard P. Feynman, Simulating physics with computers, International Journal of Theoretical Physics 21, 467 (1982).
- [2] Seth Lloyd, Universal Quantum Simulators, Science, New Series 273, 1073 (1996).

- [3] Buluta, I. and Nori, F. Quantum simulators. *Science* 326, 108111 (2009).
- [4] I. M. Georgescu, S. Ashhab, and Franco Nori., Quantum Simulation, *Rev.Mod. Phys.* 86, 153 (2014).
- [5] J. Ignacio Cirac, Peter Zoller, Goals and opportunities in quantum simulation, *Nature Physics* 8, 264 (2012).
- [6] Nature Physics Insight on Quantum Simulation. *Nat. Phys.* 8, 263299 (2012).
- [7] Laurent Sanchez-Palencia, "Quantum simulation: From basic principles to applications", arXiv:1812.01110v1.
- [8] Altman, E., *et al.* Quantum Simulators: Architectures and Opportunities, arXiv:1912.06938v1 (2019).
- [9] Immanuel Bloch, Jean Dalibard, Sylvain Nascimbene., Quantum simulations with ultracold quantum gases, *Nature Physics* 8, 267 (2012).
- [10] Alan Aspuru-Guzik, Philip Walther, Photonic quantum simulators, *Nature Physics* 8, 285 (2012).
- [11] Andrew A. Houck, Hakan E. Tiirecil, Jens Koch., On-chip quantum simulation with superconducting circuits, *Nature Physics* 8, 292 (2012).
- [12] Sarkar, S. Quantum simulation of Dirac fermion mode, Majorana fermion mode and Majorana-Weyl fermion mode in cavity QED lattice. *Euro. Phys. Lett.* 110, 64003 (2015).
- [13] Sarkar, S. Topological Quantum Phase Transition and Local Topological Order in a Strongly Interacting Light-Matter System, *Sci. Rep.* 7, 1840, DOI:10.1038/s41598-017-01726-z (2017).
- [14] L. Fu and C. L. Kane, Superconducting proximity effect and Majorana fermions at the surface of a topological insulator, *Physical Review letters*, vol. 100, no. 9, p. 096407, 2008.
- [15] Lutchyn, R. M., Sau, J. D. and Sarma, S. D. Majorana fermions and a topological phase transition in semiconductor-superconductor heterostructures. *Phys. Rev. Lett.* 105, 77001 (2010).
- [16] Oreg, Y., Refael, G. and Oppen, F. V. Helical liquids and Majorana bound states in quantum wires. *Phys. Rev. Lett.* 105, 177002 (2010).
- [17] Felix von Oppen, Yang Peng, and Falko Pientka, " Topological superconducting phases in one dimension" in *Topological Aspects of Condensed Matter Physics*. C. Chamon et al. c Oxford University Press 2017.
- [18] Kitaev, A. Y. Unpaired Majorana Fermions in Quantum Wires, *Physics-Uspekhi* 44, 131 (2001).

- [19] Wilczek, F., Majorana Returns, *Nat. Phys* **5**, 614 (2009).
- [20] J, Alicea., New directions in the pursuit of Majorana fermions in solid state systems, *Rep. Prog. Phys.* **75**, 076501 (2012).
- [21] Beenakker, C. W. J. Search for Majorana fermions in superconductors, *Annu. Rev. Condens. Matter Phys.* **4**, 113 (2013).
- [22] Kitaev, A. Y. Fault-tolerant quantum computation by anyons. *Ann. Phys.* 303, 230 (2003).
- [23] Halperin, B. I. et al. Adiabatic manipulations of Majorana fermions in a three-dimensional network of quantum wires. *Phys. Rev. B* 85, 144501 (2012).
- [24] Sau, J. D., Clarke, D. J. and Tewari, S. Controlling non-Abelian statistics of Majorana fermions in semiconductor nanowires. *Phys. Rev. B* 84, 094505 (2011).
- [25] Mourik, V. et al. Signatures of Majorana fermions in hybrid superconductor-semiconductor nanowire devices. *Science* 336, 10031007 (2012).
- [26] Deng, M. T. et al. Observation of majorana fermions in a NbInSb nanowire-Nb hybrid quantum device. Preprint at <http://arxiv.org/abs/1204.4130> (2012).
- [27] Das, A. et al. Zero-bias peaks and splitting in an AlInAs nanowire topological superconductor as a signature of Majorana fermions, *Nat. Phys.* **8**, 887 (2012).
- [28] . K. zdemir, S. Rotter, F. Nori and L. Yang Paritytime symmetry and exceptional points in photonics, *Nat. Mate* 18, 783 (2019).
- [29] Sarkar, S. Physics of Majorana modes in interacting helical liquid. *Sci. Rep.* 6, 30569; doi: 10.1038/srep30569 (2016).
- [30] Lutchyn, R. M. & Fisher, M. P. A. Interacting topological phases in multiband nanowires. *Phys. Rev. B* 84, 214528 (2011).
- [31] Lobos, A. M., Lutchyn, R. M. & Sarma, S. Interplay of Disorder and Interaction in Majorana Quantum Wires. *Phys. Rev. Lett.* 109, 146403 (2012).
- [32] Anderson, P. W. Coherent excited states in the theory of superconductivity: gauge invariance and Meissner effect. *Phys. Rev* 110, 827 (1958).
- [33] Zak, J. Berrys phase for energy bands in solids. *Phys. Rev. Lett.* 62, 2747 (1989).
- [34] Ryu, S. & Hatsugai, Y. Entangle entropy and the Berry phase in solid state. *Phys. Rev. B* 73, 245115 (2006).
- [35] Ching-Kai Chiu, Jeffrey C. Y. Teo, Andreas P. Schnyder, and Shinsei Ryu, Classification of topological quantum matter with symmetries, *Rev. Mod. Phys.*, 88, 035005 (2016).

- [36] Jorrit Kruthoff, Jan de Boer, Jasper van Wezel, Charles L. Kane, and Robert-Jan Slager, Topological Classification of Crystalline Insulators through Band Structure Combinatorics, *Phys. Rev. X.*, 7, 041069 (2017).
- [37] Liang Fu, Topological crystalline insulators, *Phys. Rev. Lett.*, 106, 106802 (2011).
- [38] Sarkar, S., Quantization of geometric phase with integer and fractional topological characterization in a quantum Ising chain with long-range interaction, *Sci Rep* DOI:10.1038/s41598-018-24136-1

Acknowledgements The author would like to acknowledge Prof. Prabir Mukherjee, Prof. R. Srikanth and Prof. M. Kumar for reading the manuscript critically. The author also would like to acknowledge RRI library, DST for books/journals and academic activities of ICTS/TIFR.

Competing interests

The author declares no competing interests.

Additional information Correspondence and requests for materials should be addressed to S.S.